Heliyon 9 (2023) e19021

Contents lists available at ScienceDirect

Heliyon

journal homepage: www.cell.com/heliyon

Nanocatalytic performance of pectinase immobilized over in situ prepared magnetic nanoparticles

Diego E. Navarro-López [a], Alvaro R. Bautista-Ayala [a], Maria Fernanda Rosales-De la Cruz [a], Selina Martínez-Beltrán [a], Diego E. Rojas-Torres [a], A. Sanchez-Martinez [b], O. Ceballos-Sanchez [c], J.A. Jáuregui-Jáuregui [a], Luis Marcelo Lozano [a], M. Sepúlveda-Villegas [d,e], Naveen Tiwari [f,**], Edgar R. López-Mena [a,*]

[a] *Tecnologico de Monterrey, Escuela de Ingeniería y Ciencias, Av. Gral Ramón Corona No. 2514, Colonia Nuevo México, 45201, Zapopan, Jalisco, Mexico*

[b] *CONACyT-Unidad Académica de Ciencias Químicas, Universidad Autónoma de Zacatecas, Campus Siglo XXI, Carretera Zacatecas - Guadalajara Km 6, Ejido La Escondida, Zacatecas, 98160, Mexico*

[c] *Universidad de Guadalajara, Centro Universitario de Ciencias Exactas e Ingenierias (CUCEI), Departamento de Ingenieria de Proyectos, Av. Jose Guadalupe Zuno #48, Industrial Los Belenes, Zapopan, Jalisco, 45157, Mexico*

[d] *Departamento de Biología Molecular y Genómica, Hospital Civil de Guadalajara, "Fray Antonio Alcalde", Guadalajara, 44280, Jalisco, Mexico*

[e] *Departamento de Biología Molecular y Genómica, Centro Universitario de Ciencias de la Salud, Universidad de Guadalajara, Guadalajara, 44100, Jalisco, Mexico*

[f] *Center for Research in Biological Chemistry and Molecular Materials (CiQUS), University of Santiago de Compostela, Rúa Jenaro de La Fuente S/N, 15782, Santiago de Compostela, A Coruna, Spain*

ARTICLE INFO

Keywords:
Pectinase
Enzyme immobilization
Magnetic nanoparticles
Cross-linking

ABSTRACT

Immobilization of enzymes is one of the protein engineering methods used to improve their thermal and long-term stabilities. Immobilized pectinase has become an essential biocatalyst for optimization in the food processing industry. Herein, nanostructured magnetic nanoparticles were prepared in situ for use as supports to immobilize pectinase. The structural, morphological, optical and magnetic features and the chemical compositions of the nanoparticles were characterized. Nanoparticle agglomeration and low porosity were observed due to the synthetic conditions. These nanoparticles exhibited superparamagnetic behavior, which is desirable for biotechnological applications. The maximum retention rate for the enzyme was observed at pH 4.5 with a value of 1179.3 U/mgNP (units per milligram of nanoparticle), which was equivalent to a 65.6% efficiency. The free and immobilized pectinase were affected by the pH and temperature. The long-term instability caused 40% and 32% decreases in the specific activities of the free and immobilized pectinase, respectively. The effects of immobilization were analyzed with kinetic and thermodynamic studies. These results indicated a significant affinity for the substrate, a decreased reaction rate, and improved thermal stability of the immobilized pectinase. The reusability of the immobilized pectinase was preserved effectively during cycling, with only a 21.2% decrease in activity observed from the first to the last use. Therefore, alternative magnetic nanoparticles are presented for immobilizing and maintaining the thermostability of pectinase.

* Corresponding author.
** Corresponding author.
E-mail addresses: naveen.tiwari@usc.es (N. Tiwari), edgarl@tec.mx (E.R. López-Mena).

https://doi.org/10.1016/j.heliyon.2023.e19021
Received 13 June 2023; Received in revised form 4 August 2023; Accepted 7 August 2023
Available online 7 August 2023

1. Introduction

Enzymes are macromolecular proteins that accelerate biochemical reactions [1]. They are classified into various categories according to their molecular activities, such as oxidoreductases, transferases, hydrolases, lyases, isomerases, and ligases [2]. Pectinase is an enzyme that breaks down pectin, a complex carbohydrate found in the cell walls of plants [3]. In the food industry, pectinase is used to improve the textures and clarities of fruit juices, wine, and beer via removal of haze-causing proteins and polysaccharides [4,5] as well as in the production of jams and jellies to disintegrate pectin and create a smoother consistency [6].

For industrial application, the lack of reusability and enzyme instability must be overcome, since they result in higher production costs [7]. Different protein engineering technologies, such as stereoselectivity, chemoselectivity, and regioselectivity, have been developed to optimize long-term stability [8]. Immobilization can address these challenges by linking the enzyme to a support matrix to ensure improved performance, rapid recovery, and reutilization [9]. Enzyme immobilization has been used successfully for several decades [10]. However, in the twenty-first century, new matrixes and methods are still required to enhance the catalytic capabilities of enzymes. These qualities, which provide better yields of the intended products, include selectivity, specificity, and decreased inhibition [11]. According to the literature, nanoparticles are used as improved immobilization matrixes due to their high surface areas and high mass transfer capacities, and they are easily recovered by applying a magnetic field [12].

A decline in enzymatic activity can be avoided by using the immobilization procedure, which consists of adsorption, covalent bonding, cross-linking, and nanoparticle immobilization. Literature reports indicate that when an enzyme is attached to a nanoparticle surface in an aqueous medium, the enzymatic activity is enhanced due to the Brownian motions of the nanoparticles. The collisions created by these movements could increase the reaction rates [13,14]. Moreover, magnetic nanoparticles have been researched to reuse enzymes due to their biocompatibility [15]. However, the residual activity of the immobilized enzyme can be affected by enzyme inactivation after the recycling process [16]. Numerous enzymes have been immobilized on Fe_3O_4, including cholesterol oxidase, laccase, amylase, lipase, and pectinase [17,18]. However, nanoparticle enzyme-based systems have been applied in a variety of processes, including the production of biofuels, bioremediation, and starch degradation, among others [19–21]. The magnetic-chitosan system has attracted interest for decades due to its versatility and broad application range. Because of its high magnetic susceptibility and saturation magnetization, Fe_3O_4 (magnetite) is the most frequently utilized magnetic material in biotechnology and related fields [22,23]. However, as an alternative to magnetite, Fe_2O_3 (ferric oxide) is an ideal material for the biomedical and biotechnology sectors. γ-Fe_2O_3 (maghemite) is one of the four polymorphic forms of ferric oxide. Maghemite has mainly been employed in medical treatments, with applications including magnetic hyperthermia, *in vitro* diagnostics, and drug delivery [24,25]. Additionally, the Food and Drug Administration (FDA) of the United States and Europe has approved the use of superparamagnetic nanoparticles for these purposes [26]. Immobilized enzymes are used as sweeteners (D-glucose), antioxidants (lipase B), and cocoa butter equivalents (lipase from RM), among other applications [27].

This study employed an innovative approach to create superparamagnetic nanobiocatalysts directly within a chitosan matrix. Extensive characterization was conducted to evaluate the structural, morphological, magnetic, and optical properties of these nanobiocatalysts. Subsequently, these nanoparticles were utilized to immobilize pectinase, and the impacts of various factors, such as the pH, temperature, time, and reusability, were investigated. Through kinetic and thermodynamic analyses, valuable insights were obtained into the nanocatalytic activity resulting from the synthetic process. The comprehensive findings obtained from this research underscore the remarkable potential for use of synthesized magnetic nanoparticles as an exceptionally effective support matrix for pectinase in the fruit processing industry.

2. Experimental section

2.1. Materials

Chitosan (M_w = 190–310 kDa, deacetylation degree of 75–85%), iron (III) chloride hexahydrate (FeCl3·6H2O), iron (II) chloride hexahydrate (FeCl2·6H2O), glutaraldehyde (GA, $OHC(CH_2)_3CHO$, 25% v/v), ammonium hydroxide solution (NH_4OH, 25 wt%), methanol (CH_4O), acetic acid (CH_3CO_2H), hydrogen peroxide solution (H_2O_2, 30% w/w), sodium hydroxide (NaOH), 3-APTES ($H_2N(CH_2)_3Si(OC_2H_5)_3$), pectinase, monobasic potassium phosphate (KH_2PO_4), dibasic potassium phosphate (K_2HPO_4), 3,5-dinitrosalicylic acid ($(O_2N)_2C_6H_2$-2-$(OH)CO_2H$) and Bradford's reagent were obtained from Sigma–Aldrich.

2.2. Synthesis of the magnetic nanoparticles

The magnetic nanoparticles (labeled MNPs) were prepared in two steps. First, 3 g of chitosan was dissolved in 100 mL of a 2% (v/v) acetic acid solution with continuous stirring. Subsequently, 0.4 mL of a 25% glutaraldehyde (GA) solution was added. After 24 h, a chitosan hydrogel was formed. In the second step, 8.34 g of $FeCl_3$ and 3.08 g of $FeCl_2$ were dissolved in 100 mL of deionized water, and the pH was adjusted to 1 with HCl. This solution was added to the hydrogel. Next, 100 mL of a NaOH solution (1.25 mol/L) was added to provide the magnetic nanoparticles. Finally, 100 mL of 8% (v/v) H_2O_2 in acetic acid was added to the degraded chitosan. The MNPs were separated by magnetic decantation after several washes with deionized water until the pH became neutral (pH 7). However, Fe_3O_4 nanoparticles are unstable and prone to oxidation. Therefore, the MNPs were calcined in air to form maghemite (γ-Fe_2O_3), which was stable [28]. The following Eq. (1) and Eq. (2) describe the process:

$$Fe^{+3} + Fe^{+2} \xrightarrow{8OH^-} Fe_3O_4 + 4H_2O \quad (1)$$

$$Fe_3O_4 + 2H^+ \rightarrow \gamma - Fe_2O_3 + Fe^{+2} + H_2O \quad (2)$$

2.3. Nanoparticle characterization

The crystal structure of the MNP powder was characterized by X-ray diffraction (XRD) using an Empyrean diffractometer (PANalytical) with a Cu anode ($\lambda = 1.5406$ Å). The XRD patterns were obtained from 20° to 60° (2θ) with a 0.01° step size. Attenuated total reflection Fourier transform infrared (ATR-FTIR) spectroscopy was employed to assess the presence of organic matter in the MNPs. ATR-FTIR spectra were recorded in the 4000–400 cm^{-1} range using an IRAffinity-1S (Shimadzu) spectrometer. The morphology of the MNPs was investigated with field emission scanning electron microscopy (FESEM, Hitachi, SU3500) operated at 15 kV and equipped with an Aztec X-Max (Oxford) energy dispersive X-ray spectrometry (EDS) system. The specific surface areas (SBET) were determined with the Brunauer–Emmett–Teller (BET) method and a Nova 4200e system (Quantachrome). The magnetic properties of the nanoparticles were determined with a Physical Properties Measurement System MS2024 (Mettler) in a mode-vibrating sample magnetometer (VSM) with applied fields of −20.0 to 20.0 kOe at room temperature. The optical properties were investigated with absorption spectra obtained with a Cary-5000 UV–vis (Agilent Technologies) spectrometer equipped with a polytetrafluoroethylene (PTFE) integration sphere. X-ray photoelectron spectroscopy (XPS) (Thermo Scientific, K-Alpha) was performed with a monochromatic Al Kα source ($h\nu = 1486$ eV) to determine the bonding states of the MNPs. All spectra were calibrated with the C 1s signal at 284.8 eV, which was produced by adventitious carbon. The Fe 2*p* and O 1s core levels were determined at 90° with a pass energy of 15 eV.

2.4. Functionalization of the magnetic nanoparticles

One gram of the MNPs was ultrasonicated in 50 mL of methanol for 1 h. After that, 3 mL of ammonium hydroxide (25 wt%) was added and ultrasonicated for 30 min. Then, 2 mL of 3-APTES was incorporated, and the solution was kept under continuous stirring at 50 °C for 9 h under reflux to prevent methanol evaporation. The MNPs were recovered with magnetic decantation and washed with deionized water until the pH became neutral.

2.5. Pectinase immobilization and activity assay

Enzymatic coupling and glutaraldehyde crosslinking were used to immobilize pectinase. The MNPs were incubated with 3% glutaraldehyde (GA) for 4 h, washed with distilled water three times, and separated by magnetic decantation (Scheme 1). The resulting MNPs were incubated at different pHs (4.5, 5, 6, 7, and 8) at 30 °C for 24 h with 1800 units of pectinase enzyme and stirring at 150 rpm. The MNPs-pectinase nanocatalyst was separated with a magnet and used for total protein quantification with the Bradford assay. The retention percentage was calculated based on the free protein before and after immobilization, and MNPs-pectinase was subjected to enzyme analysis. The pectinase activity was determined by spectrophotometrically measuring the D-galacturonic acid liberated from pectin at 595 nm with dinitrosalicylic acid. The effect of pH (4–8) at 30 °C, time (0–120 h) at 30 °C, temperature (25–55 °C), and reusability of the free and immobilized enzyme were analyzed separately by incubation at 30 °C.

3. Results and discussion

3.1. Structural and morphological characterization of the MNPs

The XRD patterns of the MNPs prepared in situ are shown in Fig. 1a. The peaks at 30°, 35°, 39°, 43°, 53°, and 57° corresponded to the (220), (311), (321), (400), (422), and (511) planes, which were consistent with JCPDS card No. 39–1346 for γ-Fe_2O_3. The XRD pattern showed broad diffraction peaks, indicating the formation of nanoparticles. The crystal system of γ-Fe_2O_3 is cubic with lattice

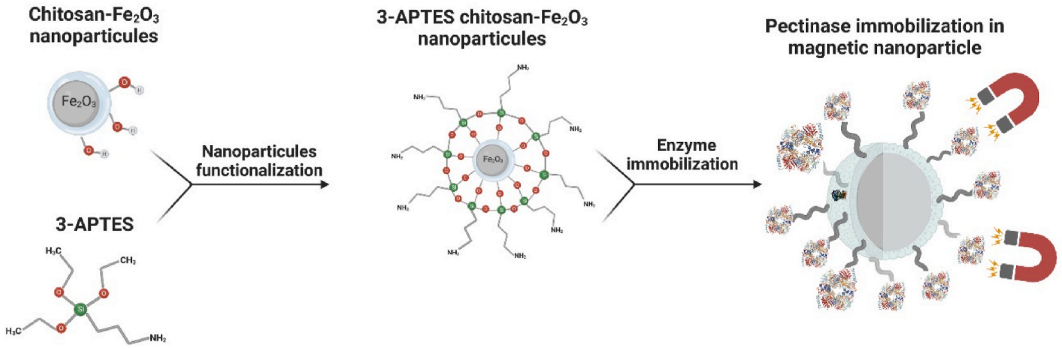

Scheme 1. Schematic representation of pectinase immobilization on magnetic nanoparticles.

parameters a = b = c = 8.29 Å, α = β = γ = 90°, and space group $P4_132$. The average crystallite size was calculated using Scherrer's formula [29], resulting in 10 ± 2 nm. These results were evaluated with the position of the diffraction peak of the (311) plane.

FTIR spectroscopy was used to determine the functional groups present in pure chitosan and the MNPs (Fig. 1b). The absorption bands for chitosan appeared at ~3274 cm^{-1} (O–H, N–H stretching vibrations), ~2923 cm^{-1} (C–H, stretching vibrations), ~1651 to 1541 cm^{-1} (N–H, bending vibrations), ~1430 cm^{-1} (C–O stretching vibration), ~1362 cm^{-1} (C–N, stretching) and ~1060 cm^{-1} (C–*O*–C, stretching vibrations) [30,31]. For the MNPs, the peak at 585 cm^{-1} was related to the Fe–O bond [32]. Strong absorption bands were located at ~1574 cm^{-1}, ~1398 cm^{-1}, and ~1024 cm^{-1}, which corresponded to the amide II peak and –CH, and $–CH_3$ peaks for the epoxy groups of GA. Additionally, FE-SEM and EDS were used to determine the morphology and composition of the MNPs (Fig. 1c). An acetic acid/H_2O_2 solution was used to break down the chitosan, as described in the synthetic process. Specific chitosan residues persisted on the nanoparticle surfaces (Fig. 1b). The chitosan matrix was primarily responsible for the aggregated MNPs, as seen from the high-magnification FESEM image (Fig. 1c). The average grain size was calculated in 29 ± 5 nm (inset Fig. 1C, grain size distribution). Fe, O, and C were found in the sample, as seen in the EDS layered picture and individual maps (Fig. 1d), which depicted uniform distributions of Fe and O and some traces of C at this level. Finally, the EDS spectrum (Fig. 1e) showed an elemental composition of Fe (52.1%), O (26.3%), and C (21.6%).

Fig. 2 shows the N_2 adsorption and desorption isotherms and (insets) the pore-size distributions of the MNPs and pectinase-MNPs. Fig. 2a demonstrates that the base material, i.e., without pectinase, exhibited type IV N_2 adsorption and desorption isotherms, as per the International Union of Pure and Applied Chemistry (IUPAC) classification [33]. These isotherms suggested the absence of a discernible monolayer, indicating that the adsorbed molecules formed clusters around the most favorable surface sites. The specific surface area of the base material was determined to be 31.15 m^2/g based on the BET method. The samples exhibited type H3 hysteresis loops predominantly, indicating that wedge-shaped pores were the primary pores present in the sample. Fig. 2a (inset) shows the pore size distribution based on the Barrett–Joyner–Halenda (BJH) model. A narrow pore size distribution with a maximum peak at approximately 3 nm indicated that the sample was a microporous and mesoporous material. Fig. 2b shows the adsorption-desorption isotherm and pore-size distribution (inset) of the material containing pectinase. There was no noticeable difference with respect to the base material without pectinase (SBET = 31.2 m^2/g).

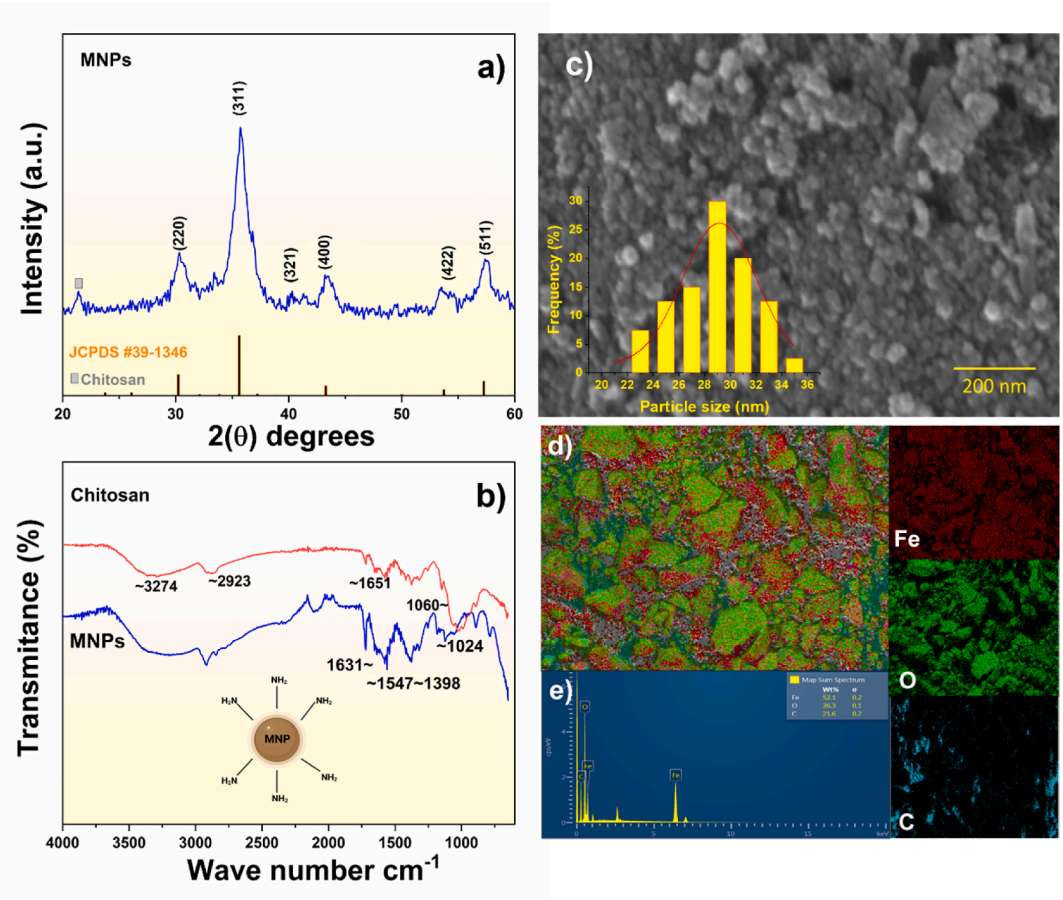

Fig. 1. Structural and morphological characterization of the MNPs and chitosan; a) XRD pattern, b) FTIR spectra, c) FE-SEM image, d) EDS layered image, e) EDS spectrum and elemental maps of the MNPs.

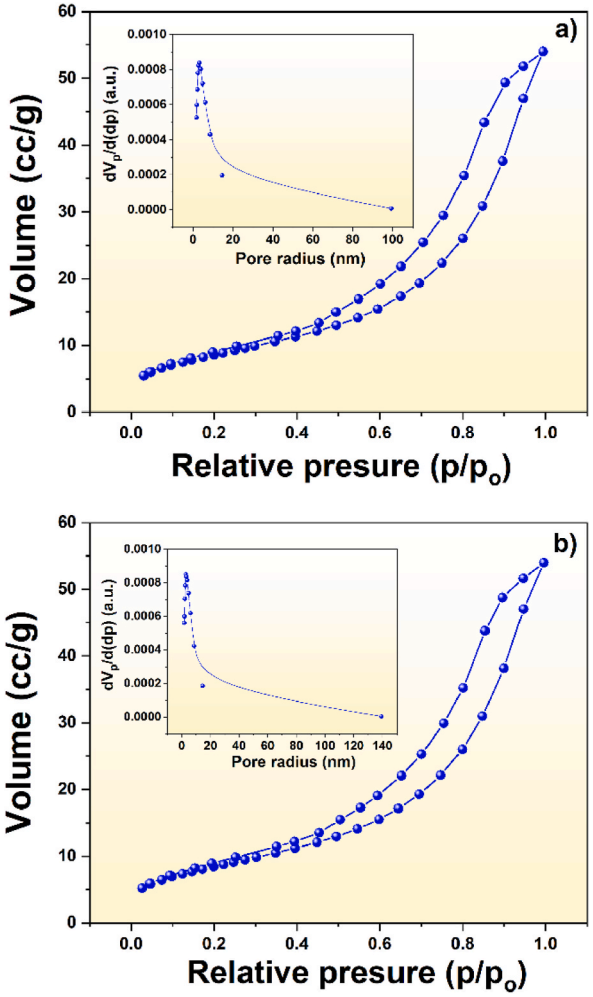

Fig. 2. Nitrogen adsorption and desorption isotherms and (inset) pore-size distributions of the a) MNPs and b) pectinase-MNPs.

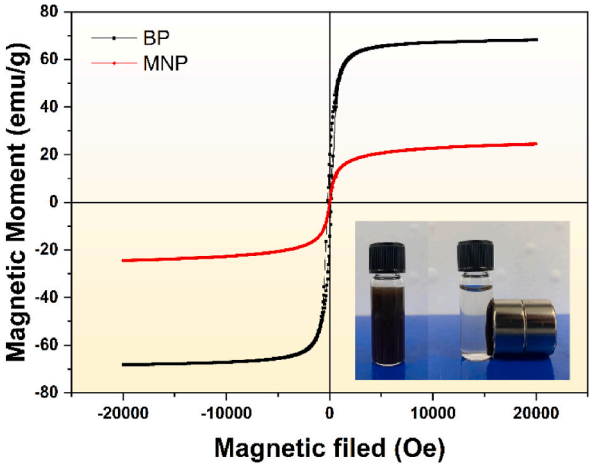

Fig. 3. Magnetic hysteresis curve for the as-prepared MNPs and bare nanoparticles.

3.2. Magnetic properties of the MNPs

The magnetic properties of the MNPs and bare nanoparticles (BP) were determined by VSM at room temperature (Fig. 3). The mass saturation magnetization (M_s) of the MNPs was 22.7 emu/g, which was than the 67.02 emu/g observed for the bare nanoparticles. The decreased M_s value was due to the presence of nonmagnetic materials, such as carbon, which weakened the magnetic properties. The magnetization curves for the bare and in situ prepared nanoparticles did not exhibit hysteresis, which was consistent with formation of the superparamagnetic material required for biotechnological and medical applications. The MNP suspension is shown in the inset (Fig. 3) both before and after exposure to an external magnet, which indicated the potential for reuse of the MNPs and demonstrated their sustainability.

3.3. Optical properties of the MNPs

UV–visible absorption spectroscopy was utilized to analyze the optical properties of chitosan and the MNPs (Fig. 4). The band gap (Eg) of the MNPs was computed from the absorbance information with the Kubelka-Munk function according to Tauc's relation. The values measured for the MNPs and chitosan were Eg = 2.15 eV and Eg = 3.1 eV, respectively, which were consistent with previously published values. Due to the lack of conjugated double bonds in the chitosan structure, the sample did not exhibit absorbance bands in the 420–1200 nm region [34]. In addition, the MNPs displayed substantial visible-wavelength absorption (Fig. 4a). The maximum absorbance wavelength was related to the $\pi \rightarrow \pi^*$ transition of C]O groups [35]. Based on the E_g value for the MNPs, the relative energies of the valence band (VB) and conduction band (CB) were calculated [36], and the values were 0.3 and 2.44 eV, respectively (Fig. 4b).

3.4. Surface analyses with X-ray photoelectron spectroscopy

Fig. 5 shows the low- and high-resolution XPS spectra for the MNPs. Fig. 5a displays the spectrum from which it was possible to

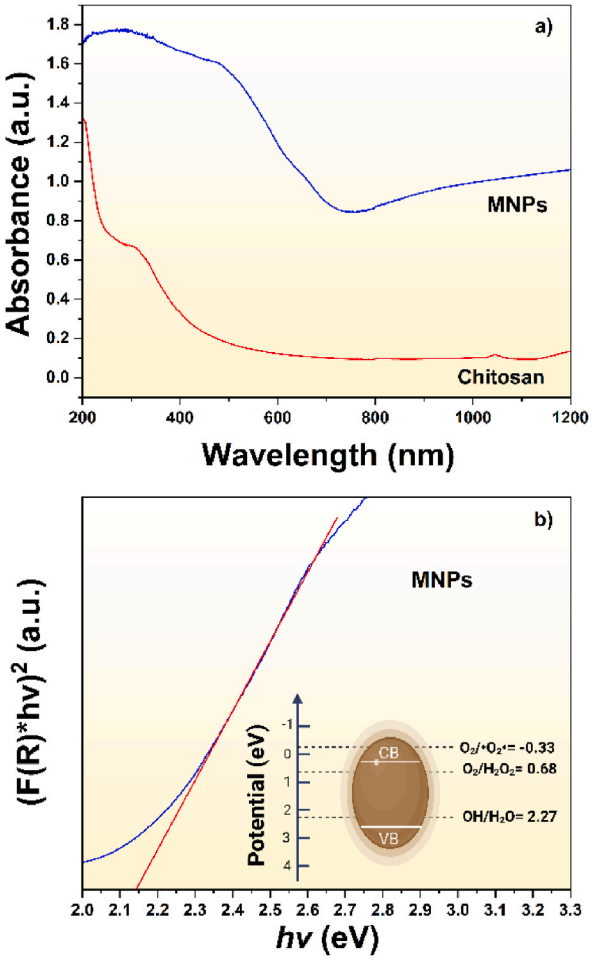

Fig. 4. a) UV–Vis absorption spectra for chitosan and the MNPs and b) band gaps estimated with the Kubelka-Munk function.

observe peaks related to the different core levels of the elements present in the sample. The presence of iron (Fe) and oxygen (O) was consistent with the elemental composition of the MNPs. The presence of carbon could be associated with organic residues from the synthetic process or adventitious carbon due to exposure of the sample to the environment. The high-resolution XPS spectra were deconvolved using Analyzer software to determine the chemical states on the nanoparticle surface [37]. In particular, the Fe 2p core level showed a stepped background and complex characteristics that were difficult to deconvolute (Fig. 5b). However, through proper background analysis, it was possible to identify the chemical components and the oxidation states of iron. A Shyrley-type background enabled reproduction of both sides of the Fe 2p core level. It was necessary to use four doublet peaks in fitting this region. The first two peaks, centered at 709.45 eV and 711.82 eV, were related to the Fe^{2+} and Fe^{3+} oxidation states [38]. The satellites centered at 715.0 eV and 718.95 eV were fingerprints of the Fe^{2+} and Fe^{3+} oxidation states [39]. Fig. 5c shows the O 1s core level, which was fitted with three single peaks. The first peak centered at 529.74 eV was associated with O^{2-} ions in an FeOx structure, while the peak at 531.0 eV was associated with OH radicals, and the third was associated with O–C bonds. The C 1s core level (Fig. 5d) was fitted with three single peaks, which were related to C–C bonds (284.8 eV), C–O bonds (286.38 eV), and C]O bonds (288.61 eV). The presence of the Fe^{2+} and Fe^{3+} ions confirmed the formation of Fe_2O_3 and Fe_3O_4, as revealed by the XRD analysis. However, it is worth noting that the Fe^{2+}:Fe^{3+} ratio was 2:1.

3.5. Catalytic properties of free and immobilized pectinase

The purpose of immobilizing pectinase on the surfaces of the nanoparticles was to achieve optimal conditions for industrial application of the immobilized rather than free pectinase. Parameters such as the pH, temperature, time, and reusability were studied (Fig. 6). The Fourier transform infrared (FTIR) spectra of the pectinase and immobilized pectinase (IPE) are shown in Fig. 6a. The characteristic peaks for pectinase included those for the $–NH_2$ (~3500 cm^{-1}) and –COOH vibrations. The stretching vibrational bands for the carboxyl groups were observed at ~2930 (−OH) and ~1650 cm^{-1} (−C═O) in the pectinase spectrum. According to the literature, GA and the enzyme form a Schiff base with a C]N group (~1650 cm-1) [40]. Additionally, the shifted positions of the peaks for the immobilized pectinase indicated successful bonding between pectinase and the MNPs [41]. Maximum retention of the enzyme was observed at pH 4.5 with 1179.3 U/mgNP (units per milligram of nanoparticle) (Fig. 6b). The strongest catalytic performance occurred under strongly acidic conditions for the free and immobilized pectinase, specifically at a pH of 5 (Fig. 6c). Beyond this pH, the

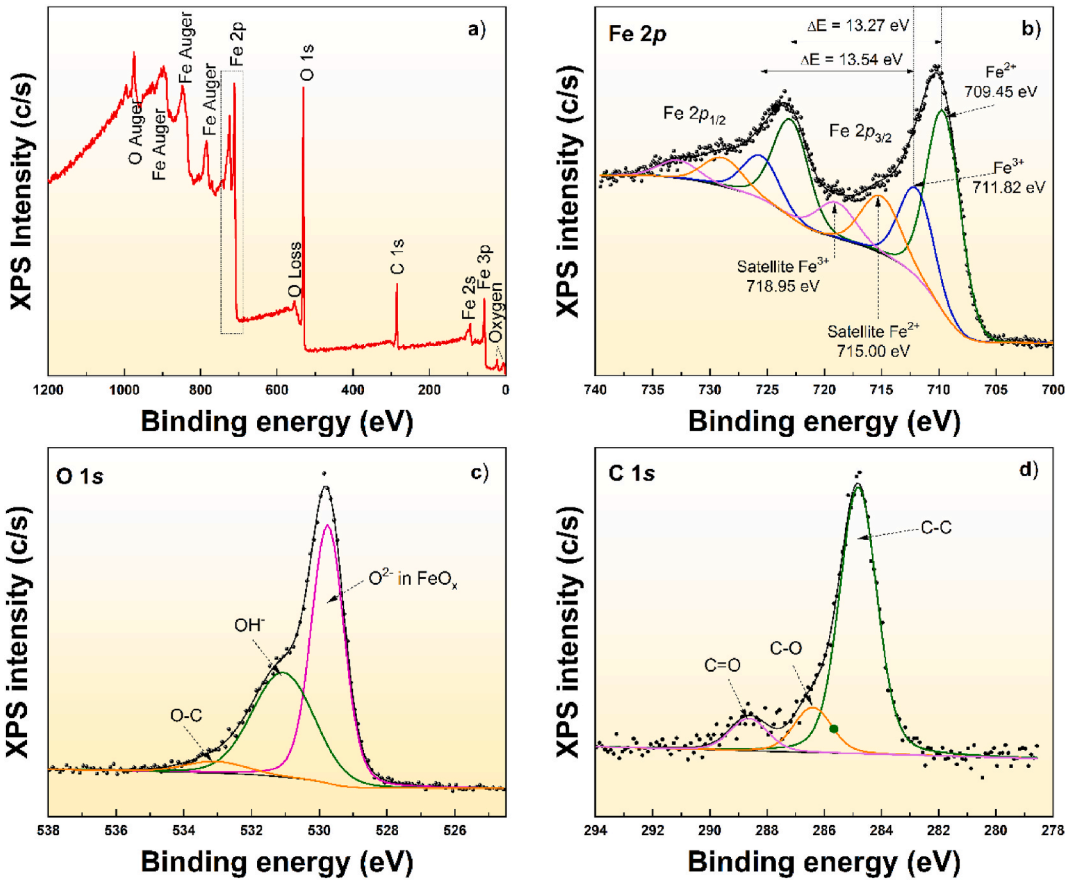

Fig. 5. a) XPS spectra of the MNPs, b) Fe 2p core level spectrum, c) O 1s core level spectrum and d) C 1s core level spectrum.

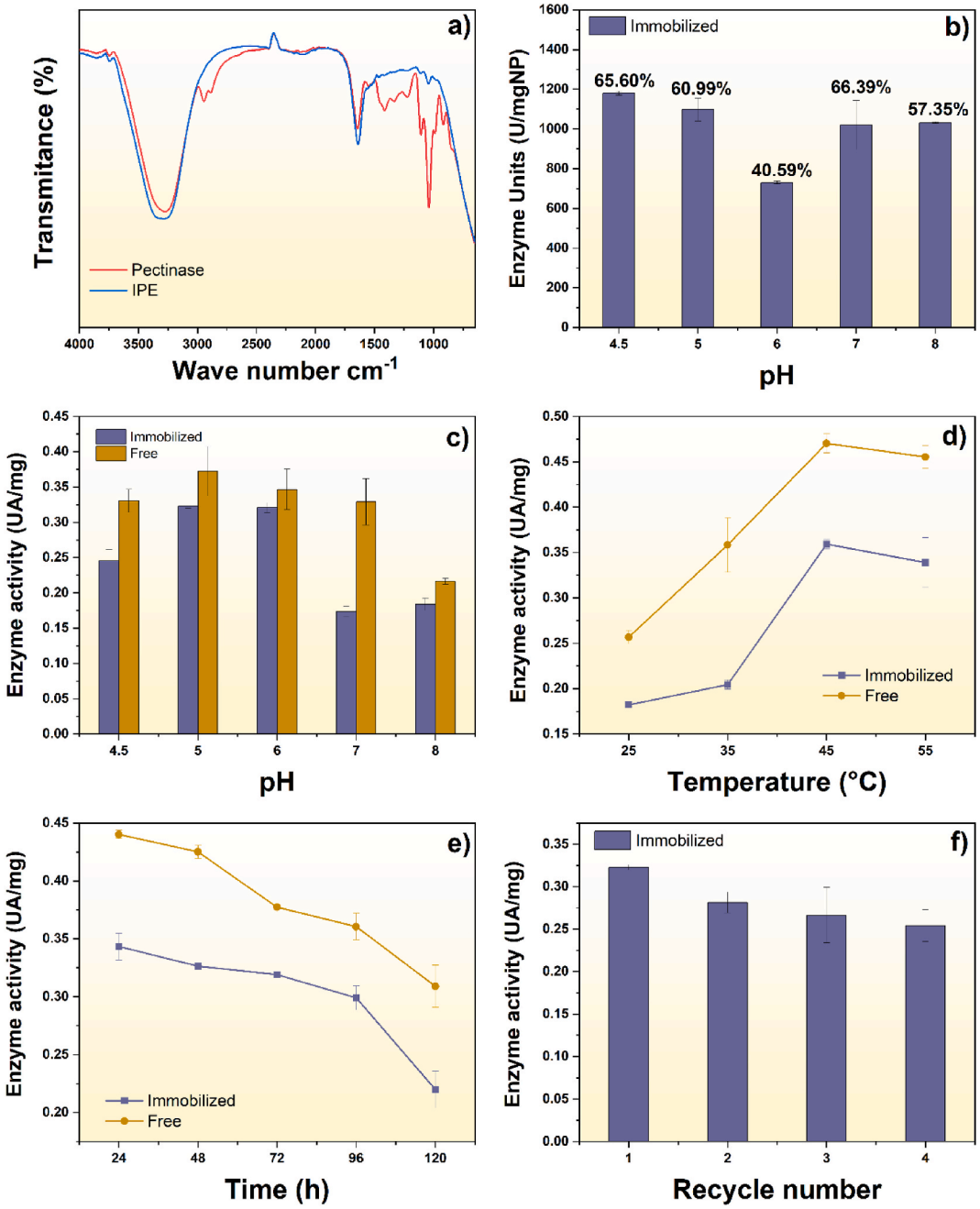

Fig. 6. Immobilization and catalytic performance of the free and immobilized pectinase; a) FTIR spectra, b) enzyme retained expressed as units per milligram of nanoparticles (U/mgNP), c) effect of pH, d) effect of temperature, d) effect of time and e) reusability of the immobilized pectinase expressed as enzyme activity (U/mg).

specific activity of the free pectinase gradually decreased to 0.184 UA/mg at pH 8. However, the immobilized pectinase retained its maximum specific activity at pH 5 and 6 (0.32 UA/mg). Beyond these values, the activity dropped to nearly 50% lower than that at pH 5. The free pectinase displayed higher specific activity across a wider range of pH values than the immobilized pectinase, indicating that the activities of both enzymes were affected by the pH. When comparing the activities of enzymes, thermal stability is a crucial consideration. A temperature range of 25 °C–55 °C was used in this analysis (Fig. 6d). Free and immobilized pectinase exhibited maximum activities at 45 °C (0.47 and 0.35 UA/mg, respectively). The activity of the free enzyme at 45 °C was almost double that seen at room temperature. However, at 55 °C, this activity fell by 5%. Similar behavior was seen with the immobilized enzyme. Again, the activity increased at all temperatures examined when free pectinase was present. The long-term stabilities of the free and immobilized enzymes were analyzed over 120 h (Fig. 6e). The specific activity of the free pectinase decreased by 40% from the initial value. In

contrast, the immobilized pectinase showed a reduction of 32%. The reusability of an enzyme in an industrial process reduces the production costs. However, reutilization of the free pectinase was not possible. Instead, the specific activity of the immobilized pectinase was reduced by only 20% after 4 cycles (from 0.32 to 0.25 UA/mg) (Fig. 6f).

3.6. Effects of immobilization on the kinetic and thermodynamic parameters of pectinase

The kinetic parameters for the free and immobilized pectinase were determined at pH 5 and 30 °C using the Lineweaver–Burk model [42]:

$$\frac{1}{v_0} = \frac{K_m}{V_{max}}\left(\frac{1}{S}\right) + \frac{1}{V_{max}} \tag{3}$$

where v_0 is the initial velocity of an enzyme reaction, K_m is the Michaelis constant, $V_{\max}$ is the maximum velocity of the reaction, and S is the substrate concentration. From Eq. (3), the obtained values for the immobilized enzyme were $V_{\max} = 0.41$ U/mg and $K_m = 6.52$ g/L, and for the free enzyme $V_{\max} = 1.07$ U/mg and $K_m = 17.65$ g/L. The decrease in K_m for the immobilized enzyme indicated a higher substrate affinity [43]. The observed increase in the substrate affinity could have resulted from better access to the active sites facilitated by immobilization [44]. On the other hand, the lower value of $V_{\max}$ in the case of the immobilized enzyme was associated with stronger diffusional restrictions, i.e., the reaction could become a diffusion-limited process after immobilization. This is principally related to the structure (agglomerated nanoparticles), as shown with FE-SEM.

The thermal stabilities of the free and immobilized pectinase were analyzed at 36 °C for 120 h, and the kinetic and thermodynamic parameters were calculated. Based on the Arrhenius method, the deactivation energy (Eq. (4)) was obtained with the following equation [45]:

$$k_d = Ae^{\frac{-E_d}{RT}} \tag{4}$$

where k_d is the deactivation rate constant, A is a constant, E_d is the deactivation energy, R (8.314×10^{-3} kJ mol^{-1} K^{-1}) is the universal gas constant, and T is the absolute temperature. The time required for the enzyme to show a decrease to 50% of the initial activity (half-life) is $t_{1/2} = \ln 2/k$. With the value of $t_{1/2}$ for immobilized/free enzyme, it was possible to obtain the stabilization factor (SF). The thermodynamic parameters for both pectinases were calculated as follows [46]:

$$\Delta H^* = E_d - RT \tag{5}$$

$$\Delta G^* = -RTln\left(\frac{k_d h}{k_B T}\right) \tag{6}$$

$$T\Delta S = \Delta H^* - \Delta G^* \tag{7}$$

where h (6.6262×10^{-34} Js) is the Planck constant and k_B (1.3806×10^{-23} JK^{-1}) is the Boltzmann constant. The results are shown in Table 1.

The kinetic and thermodynamic data for the enzyme thermal deactivation process indicated an increase in the thermostability of the enzyme after immobilization. The half-life of the deactivation reaction increased from 121.6 to 157.53 h, thus increasing the SF by 30%, which established a slower thermal deactivation process for the immobilized enzyme. Regarding the thermodynamic parameters, Table 1 shows that ΔG* (Eq. (6)) increased slightly from 102.54 to 103.22 kJ/mol for the immobilized enzyme. This demonstrated that immobilization improved the thermal stability of the enzyme, making it more resistant to denaturation and conformational changes [47]. As seen in Eq. (7) and Table 1, ΔG* was positive because ΔH* (Eq. (5)) was also positive and ΔS* was negative, and both contributed to the stability of the enzyme after immobilization. While ΔS* remained virtually unchanged after immobilization, ΔH* showed a slight increase, demonstrating higher stability due to van der Waals-type interactions or hydrogen bonds [48].

4. Conclusion

MNPs were efficiently prepared in situ from a chitosan matrix, and their structural, morphological, and optical properties were characterized. These MNPs were then functionalized and utilized as a support to immobilize pectinase. The immobilized pectinase demonstrated enhanced affinity for the substrate and a lower reaction rate compared with free pectinase. However, the immobilized enzyme specific activity was lower than that of the free enzyme. This discrepancy was attributed to the distribution of nanoparticles and the insolubility of the MNPs, resulting in colloidal properties that caused the immobilized enzyme to settle at the bottom of the reaction tube. Consequently, there were reduced interactions between the immobilized enzyme and the substrate. Nonetheless, the pectinase immobilization process led to improved thermostability.

Author contribution statement

Diego Eloyr Navarro-López, Naveen Tiwari, Edgar R. López Mena: conceived and designed the experiments, performed the experiments, analyzed and interpreted the data, contributed reagents, materials, analysis tools or data, wrote the paper.

Table 1
Thermal inactivation and thermodynamic parameters for free and immobilized pectinase.

Parameter	Free pectinase	Immobilized pectinase
K_m (g/L)	1.07	0.41
V_{max} (U/mg)	17.65	6.52
k_d (h^{-1})	0.0057	0.0044
$t_{1/2}$ (h)	121.60	157.53
SF	–	1.30
ΔG* (kJ/mol)	102.54	103.22
ΔH* (kJ/mol)	21.84	22.52
ΔS* (kJ/mol)	−0.253	−0.254

Alvaro R. Bautista-Ayala, Maria Fernanda Rosales-De la Cruz, Selina Martínez-Beltrán, Diego E. Rojas-Torres, M. Sepúlveda-Villegas: performed the experiments, analyzed and interpreted the data.

A. Sanchez-Martinez, O. Ceballos-Sanchez, Luis Marcelo Lozano, J. A. Jáuregui-Jáuregui: analyzed and interpreted the data, contributed reagents, materials, analysis tools or data, wrote the paper.

Data availability statement

Data will be made available on request.

Declaration of competing interest

The authors declare that they have no known competing financial interests or personal relationships that could have appeared to influence the work reported in this paper.

Acknowledgements

Alvaro R. Bautista-Ayala, M. Fernanda Rosales-De la Cruz, Selina Martínez-Beltrán, and Diego E. Rojas-Torres acknowledge Tecnologico de Monterrey for their undergraduate scholarship. This work was partially funded by Tecnológico de Monterrey, through the Challenge-Based Research Funding Program (Project ID: E090-EIC-GI04 -A-T3-E) and Nanodevices Research Groups. A. Sanchez-Martinez acknowledges CONACyT Mexico through the Catedras-CONACyT # 67 project. O. Ceballos-Sanchez thanks the Universidad de Guadalajara Mexico for the PRO–SNI–2022 project and CONACyT Mexico through CF2021-316883 Project.

References

[1] S. Martínez Cuesta, S.A. Rahman, N. Furnham, J.M. Thornton, The classification and evolution of enzyme function, Biophys. J. 109 (2015) 1082–1086, https://doi.org/10.1016/j.bpj.2015.04.020.
[2] A.G. McDonald, K.F. Tipton, Fifty-five years of enzyme classification: advances and difficulties, FEBS J. 281 (2014) 583–592, https://doi.org/10.1111/febs.12530.
[3] S. Satapathy, J.R. Rout, R.G. Kerry, H. Thatoi, S.L. Sahoo, Biochemical prospects of various microbial pectinase and pectin: an approachable concept in pharmaceutical bioprocessing, Front. Nutr. 7 (2020), https://doi.org/10.3389/fnut.2020.00117.
[4] L. Dal Magro, K.S. de Moura, B.E. Backes, E.W. de Menezes, E.V. Benvenutti, S. Nicolodi, M.P. Klein, R. Fernandez-Lafuente, R.C. Rodrigues, Immobilization of pectinase on chitosan-magnetic particles: influence of particle preparation protocol on enzyme properties for fruit juice clarification, Biotechnology Reports 24 (2019), https://doi.org/10.1016/j.btre.2019.e00373.
[5] M.R. Ladole, P.B. Pokale, V.R. Varude, P.G. Belokar, A.B. Pandit, One pot clarification and debittering of grapefruit juice using co-immobilized enzymes@chitosanMNPs, Int. J. Biol. Macromol. 167 (2021) 1297–1307, https://doi.org/10.1016/j.ijbiomac.2020.11.084.
[6] C. Lara-Espinoza, E. Carvajal-Millán, R. Balandrán-Quintana, Y. López-Franco, A. Rascón-Chu, Pectin and pectin-based composite materials: beyond food texture, Molecules 23 (2018), https://doi.org/10.3390/molecules23040942.
[7] L.J. Li, W.J. Xia, G.P. Ma, Y.L. Chen, Y.Y. Ma, A study on the enzymatic properties and reuse of cellulase immobilized with carbon nanotubes and sodium alginate, Amb. Express 9 (2019), https://doi.org/10.1186/s13568-019-0835-0.
[8] H. Gao, J. Li, D. Sivakumar, T.S. Kim, S.K.S. Patel, V.C. Kalia, I.W. Kim, Y.W. Zhang, J.K. Lee, NADH oxidase from Lactobacillus reuteri: a versatile enzyme for oxidized cofactor regeneration, Int. J. Biol. Macromol. 123 (2019) 629–636, https://doi.org/10.1016/j.ijbiomac.2018.11.096.
[9] S.A. Ansari, Q. Husain, Potential applications of enzymes immobilized on/in nano materials: a review, Biotechnol. Adv. 30 (2012) 512–523, https://doi.org/10.1016/j.biotechadv.2011.09.005.
[10] A.A. Homaei, R. Sariri, F. Vianello, R. Stevanato, Enzyme immobilization: an update, J Chem Biol 6 (2013) 185–205, https://doi.org/10.1007/s12154-013-0102-9.
[11] R.A. Sheldon, Enzyme immobilization: the quest for optimum performance, Adv. Synth. Catal. 349 (2007) 1289–1307, https://doi.org/10.1002/adsc.200700082.
[12] M. Bilal, Y. Zhao, T. Rasheed, H.M.N. Iqbal, Magnetic nanoparticles as versatile carriers for enzymes immobilization: a review, Int. J. Biol. Macromol. 120 (2018) 2530–2544, https://doi.org/10.1016/j.ijbiomac.2018.09.025.
[13] S. Block, Brownian motion at lipid membranes: a comparison of hydrodynamic models describing and experiments quantifying diffusion within lipid bilayers, Biomolecules 8 (2018), https://doi.org/10.3390/biom8020030.
[14] A.Y. Jee, Y.K. Cho, S. Granick, T. Tlusty, Catalytic enzymes are active matter, Proc. Natl. Acad. Sci. U.S.A. 115 (2018), https://doi.org/10.1073/pnas.1814180115.
[15] S.K.S. Patel, M.Z. Anwar, A. Kumar, S.V. Otari, R.T. Pagolu, S.Y. Kim, I.W. Kim, J.K. Lee, Fe2O3 yolk-shell particle-based laccase biosensor for efficient detection of 2,6-dimethoxyphenol, Biochem. Eng. J. 132 (2018) 1–8, https://doi.org/10.1016/j.bej.2017.12.013.
[16] S.K.S. Patel, V.C. Kalia, J.K. Lee, Laccase immobilization on copper-magnetic nanoparticles for efficient bisphenol degradation, J. Microbiol. Biotechnol. 33 (2023) 127–134, https://doi.org/10.4014/jmb.2210.10032.

[17] S.V. Otari, S.K.S. Patel, V.C. Kalia, J.K. Lee, One-step hydrothermal synthesis of magnetic rice straw for effective lipase immobilization and its application in esterification reaction, Bioresour. Technol. 302 (2020), https://doi.org/10.1016/j.biortech.2020.122887.
[18] S.K.S. Patel, R.K. Gupta, S.Y. Kim, I.W. Kim, V.C. Kalia, J.K. Lee, Rhus vernicifera laccase immobilization on magnetic nanoparticles to improve stability and its potential application in bisphenol A degradation, Indian J. Microbiol. 61 (2021) 45–54, https://doi.org/10.1007/s12088-020-00912-4.
[19] A. Basso, S. Serban, Industrial applications of immobilized enzymes—a review, Mol. Catal. 479 (2019), https://doi.org/10.1016/j.mcat.2019.110607.
[20] H. Shokrollahi, A review of the magnetic properties, synthesis methods and applications of maghemite, J. Magn. Magn Mater. 426 (2017) 74–81, https://doi.org/10.1016/j.jmmm.2016.11.033.
[21] S.A. Ansari, Q. Husain, Potential applications of enzymes immobilized on/in nano materials: a review, Biotechnol. Adv. 30 (2012) 512–523, https://doi.org/10.1016/j.biotechadv.2011.09.005.
[22] B.A. Kikani, S.P. Singh, Enzyme stability, thermodynamics and secondary structures of α-amylase as probed by the CD spectroscopy, Int. J. Biol. Macromol. 81 (2015) 450–460, https://doi.org/10.1016/j.ijbiomac.2015.08.032.
[23] S.S. Salem, A. Fouda, Green synthesis of metallic nanoparticles and their prospective biotechnological applications: an overview, Biol. Trace Elem. Res. 199 (2021) 344–370, https://doi.org/10.1007/s12011-020-02138-3.
[24] H. Shokrollahi, A review of the magnetic properties, synthesis methods and applications of maghemite, J. Magn. Magn Mater. 426 (2017) 74–81, https://doi.org/10.1016/j.jmmm.2016.11.033.
[25] S. Kour, R. kumar Sharma, R. Jasrotia, V.P. Singh, A brief review on the synthesis of maghemite (?-Fe2O3) for medical diagnostic and solar energy applications, in: AIP Conf Proc, American Institute of Physics Inc., 2019, https://doi.org/10.1063/1.5122451.
[26] R. Di Corato, A. Aloisi, S. Rella, J.M. Greneche, G. Pugliese, T. Pellegrino, C. Malitesta, R. Rinaldi, Maghemite nanoparticles with enhanced magnetic properties: one-pot preparation and ultrastable dextran shell, ACS Appl. Mater. Interfaces 10 (2018) 20271–20280, https://doi.org/10.1021/acsami.7b18411.
[27] A. Basso, S. Serban, Industrial applications of immobilized enzymes—a review, Mol. Catal. 479 (2019), https://doi.org/10.1016/j.mcat.2019.110607.
[28] T. Behram, S. Pervez, M.A. Nawaz, S. Ahmad, A.U. Jan, H.U. Rehman, S. Ahmad, N.M. Khan, F.A. Khan, Development of pectinase based nanocatalyst by immobilization of pectinase on magnetic iron oxide nanoparticles using glutaraldehyde as crosslinking agent, Molecules 28 (2023), https://doi.org/10.3390/molecules28010404.
[29] J. Nanosains, Derivation of scherrer relation using an approach in, Basic Physics Course 1 (2008) 28–32.
[30] S. Kumar, J. Koh, Physiochemical, optical and biological activity of chitosan-chromone derivative for biomedical applications, Int. J. Mol. Sci. 13 (2012) 6103–6116, https://doi.org/10.3390/ijms13056102.
[31] Z. Kalaycıoğlu, E. Torlak, G. Akın-Evingür, İ. Özen, F.B. Erim, Antimicrobial and physical properties of chitosan films incorporated with turmeric extract, Int. J. Biol. Macromol. 101 (2017) 882–888, https://doi.org/10.1016/j.ijbiomac.2017.03.174.
[32] H. Liao, D. Chen, L. Yuan, M. Zheng, Y. Zhu, X. Liu, Immobilized cellulase by polyvinyl alcohol/Fe2O3 magnetic nanoparticle to degrade microcrystalline cellulose, Carbohydr. Polym. 82 (2010) 600–604, https://doi.org/10.1016/j.carbpol.2010.05.021.
[33] M. Thommes, K. Kaneko, A.V. Neimark, J.P. Olivier, F. Rodriguez-Reinoso, J. Rouquerol, K.S.W. Sing, Physisorption of gases, with special reference to the evaluation of surface area and pore size distribution (IUPAC Technical Report), Pure Appl. Chem. 87 (2015) 1051–1069, https://doi.org/10.1515/pac-2014-1117.
[34] V. Thamilarasan, V. Sethuraman, K. Gopinath, C. Balalakshmi, M. Govindarajan, R.A. Mothana, N.A. Siddiqui, J.M. Khaled, G. Benelli, Single step fabrication of chitosan nanocrystals using Penaeus semisulcatus: potential as new insecticides, antimicrobials and plant growth promoters, J. Cluster Sci. 29 (2018) 375–384, https://doi.org/10.1007/s10876-018-1342-1.
[35] N.I.M. Fauzi, Y.W. Fen, N.A.S. Omar, S. Saleviter, W.M.E.M.M. Daniyal, H.S. Hashim, M. Nasrullah, Nanostructured chitosan/maghemite composites thin film for potential optical detection of mercury ion by surface plasmon resonance investigation, Polymers 12 (2020) 1–13, https://doi.org/10.3390/polym12071497.
[36] R. Khurram, Z. Wang, M.F. Ehsan, S. Peng, M. Shafiq, B. Khan, Synthesis and characterization of an α-Fe2O3/ZnTe heterostructure for photocatalytic degradation of Congo red, methyl orange and methylene blue, RSC Adv. 10 (2020) 44997–45007, https://doi.org/10.1039/d0ra06866g.
[37] A. Herrera-Gomez, AAnalyzer: an Analysis Software for Photoelectron and Infrared Spectra, 2014. http://qro.cinvestav.mx/~aanalyzer/.
[38] T. Fujii, F.M.F. de Groot, G.A. Sawatzky, F.C. Voogt, T. Hibma, K. Okada, In situ xps analysis of various iron oxide films grown by (formula presented)-assisted molecular-beam epitaxy, Phys. Rev. B Condens. Matter 59 (1999) 3195–3202, https://doi.org/10.1103/PhysRevB.59.3195.
[39] N.S. McIntyre, D.G. Zetaruk, X-Ray photoelectron spectroscopic studies of iron oxides, Anal. Chem. 49 (1977) 1521–1529, https://doi.org/10.1021/ac50019a016.
[40] Q. Miao, C. Zhang, S. Zhou, L. Meng, L. Huang, Y. Ni, L. Chen, Immobilization and characterization of pectinase onto the cationic polystyrene resin, ACS Omega 6 (2021) 31683–31688, https://doi.org/10.1021/acsomega.1c04374.
[41] A. Soozanipour, A. Taheri-Kafrani, M. Barkhori, M. Nasrollahzadeh, Preparation of a stable and robust nanobiocatalyst by efficiently immobilizing of pectinase onto cyanuric chloride-functionalized chitosan grafted magnetic nanoparticles, J. Colloid Interface Sci. 536 (2019) 261–270, https://doi.org/10.1016/j.jcis.2018.10.053.
[42] H. Lineweaver, D. Burk, The determination of enzyme dissociation constants, J. Am. Chem. Soc. 56 (1934) 658–666, https://doi.org/10.1021/ja01318a036.
[43] C. Molina-Fernández, A. Péters, D.P. Debecker, P. Luis, Immobilization of carbonic anhydrase in a hydrophobic poly(ionic liquid): a new functional solid for CO2 capture, Biochem. Eng. J. 187 (2022), 108639, https://doi.org/10.1016/j.bej.2022.108639.
[44] F. Gashtasbi, G. Ahmadian, K.A. Noghabi, New insights into the effectiveness of alpha-amylase enzyme presentation on the Bacillus subtilis spore surface by adsorption and covalent immobilization, Enzym. Microb. Technol. 64 (65) (2014) 17–23, https://doi.org/10.1016/j.enzmictec.2014.05.006.
[45] B.C. de Andrade, A. Gennari, G. Renard, B.D.R. Nervis, E.V. Benvenutti, T.M.H. Costa, S. Nicolodi, N.P. da Silveira, J.M. Chies, G. Volpato, C.F. Volken de Souza, Synthesis of magnetic nanoparticles functionalized with histidine and nickel to immobilize His-tagged enzymes using β-galactosidase as a model, Int. J. Biol. Macromol. 184 (2021) 159–169, https://doi.org/10.1016/j.ijbiomac.2021.06.060.
[46] B.A. Kikani, S.P. Singh, Enzyme stability, thermodynamics and secondary structures of α-amylase as probed by the CD spectroscopy, Int. J. Biol. Macromol. 81 (2015) 450–460, https://doi.org/10.1016/j.ijbiomac.2015.08.032.
[47] B.C. de Andrade, A. Gennari, G. Renard, B.D.R. Nervis, E.V. Benvenutti, T.M.H. Costa, S. Nicolodi, N.P. da Silveira, J.M. Chies, G. Volpato, C.F. Volken de Souza, Synthesis of magnetic nanoparticles functionalized with histidine and nickel to immobilize His-tagged enzymes using β-galactosidase as a model, Int. J. Biol. Macromol. 184 (2021) 159–169, https://doi.org/10.1016/j.ijbiomac.2021.06.060.
[48] V.G.H. Eijsink, A. Bjørk, S. Gåseidnes, R. Sirevåg, B. Synstad, B. van den Burg, G. Vriend, Rational engineering of enzyme stability, J. Biotechnol. 113 (2004) 105–120, https://doi.org/10.1016/j.jbiotec.2004.03.026.